Hindawi Publishing Corporation
International Journal of Navigation and Observation
Volume 2015, Article ID 295029, 15 pages
http://dx.doi.org/10.1155/2015/295029

Research Article

Enhancing Weak-Signal Carrier Phase Tracking in GNSS Receivers

James T. Curran

Institute for the Protection and Security of the Citizen, European Commission's Joint Research Centre (JRC), Ispra, Italy

Correspondence should be addressed to James T. Curran; jamestcurran@ieee.org

Received 30 June 2015; Revised 29 September 2015; Accepted 20 October 2015

Academic Editor: Olivier Julien

Examining the performance of the GNSS PLL, this paper presents novel results describing the statistical properties of four popular phase estimators under both strong- and weak-signal conditions when subject to thermal noise, deterministic dynamics, and typical pedestrian motion. Design routines are developed which employ these results to enhance weak-signal performance of the PLL in terms of transient response, steady-state errors, and cycle-slips. By examining both single and data-pilot signals, it is shown that appropriate design and tuning of the PLL can significantly enhance tracking performance, in particular when used for pedestrian applications.

1. Introduction

Despite the military origins of Global Navigation Satellite Systems (GNSS), the most widespread use of GNSS receivers is civilian and the single most common receiver platform is the cellular handset. Although the civilian user is, generally, less demanding in terms of position, velocity, and timing accuracy, signal processing for civilian applications is not a simple task. Severe attenuation experienced in the indoor environment, multipath propagation through urban environments, and the limitations of consumer-grade receivers are all obstacles to maintaining acceptable receiver performance.

While many receivers can adequately track carrier frequency under most operating conditions, including in the indoor environment, reliable carrier phase tracking still proves challenging. Owing to a very short wavelength, when subject to any appreciable attenuation, the dynamics of pedestrian motion can induce carrier phase cycle-slips or even loss of phase-lock. Despite these challenges, the ability to track carrier phase is desirable for many reasons including enhanced bit-synchronization, reduced bit-error-rate, enhanced range estimation, improved velocity estimation, and, ultimately, provision for carrier-based positioning.

In response to this challenge, this paper focuses on the process of carrier phase tracking in a scalar phase-lock-loop (PLL). The primary weakness of the PLL when operating on attenuated signals is the process of phase error estimation or phase discrimination. The performance of phase discriminator functions typically degrades rapidly with reduced signal strength and their behavior under weak-signal conditions is generally unique to each discriminator function. To best design a PLL, therefore, this behavior must be understood. This work aims to develop a thorough mathematical model for the carrier phase discriminator and, from this model, to infer best practices for GNSS PLL design. In particular, two case studies are investigated: pedestrian navigation using the GPS L1 C/A signal and data-pilot tracking of the Galileo E1 B/C signal.

Two classes of phase discriminator will be examined, those which employ pure-PLL discriminators and those which employ Costas discriminators. Pure-PLL discriminators are those which are designed to capture the entire phase error on the interval $[-\pi, \pi]$ and are therefore useful for synchronization with continuous wave signals or those with smooth modulation, such as frequency-modulation. They represent the earliest form of PLL, dating back to the 1930s [1] and over the last decade have seen applications in GNSS receivers for modernized signals which include a pilot signal-component. By the 1950s, the use of suppressed-carrier modulation required the development of PLLs which were insensitive to carrier-modulation of which the most notable is

the Costas PLL [2]. This type of PLL, capturing the phase error on the interval $[-\pi/2, \pi/2]$, is widely used in GNSS receivers for BPSK modulated signals, such as GPS L1 C/A or Galileo E1B. Strictly speaking, the Costas PLL is that which performs phase estimation via the product of the in-phase and quadrature base-band channels; however, the term Costas PLL or Costas discriminator has become synonymous with the class of all modulation-insensitive phase discriminators.

The paper is organized as follows: Section 2 introduces the GNSS signal, the PLL architecture, and the linearized PLL model. A statistical analysis of four popular carrier phase estimators is developed in Section 3. Weak-signal effects on the transient and steady-state performance of the PLL are considered in Section 4 and Section 5 presents the application of the theory developed here to the problem of PLL design.

2. Receiver Model and PLL Architecture

To facilitate the following analysis, the PLL is modeled as a simplified linear, time-invariant (LTI) system. A model of the received signal and the corresponding correlator values are developed and a general description of the classical PLL is introduced. A selection of discriminator functions are examined and equivalent linear models are provided, including an assessment of the operating region over which the linearization is accurate. These component models are then combined to yield a linearized system describing the PLL operation. Through these models, it is proposed that the PLL behavior under weak-signal conditions can be described as the superposition of the response of an equivalent linear model of the PLL to various stimuli, including that of thermal noise and of phase variations, where the particular linear model is a function of the prevailing signal strength.

2.1. Downconversion and IF Signal Processing. The correlation of the local replica signals with the incoming digital intermediate frequency (IF) signal over the interval $[(m-1)T_L : mT_L]$ can be approximated by the well-known expressions for the in-phase, I, and quadrature, Q, values [3, 4]:

$$\begin{aligned} I &= \sqrt{C} d R(\tau)\, \mathrm{sinc}\left(\frac{\delta\omega T_L}{2}\right)\cos(\delta\theta) + n_i, \\ Q &= \sqrt{C} d R(\tau)\, \mathrm{sinc}\left(\frac{\delta\omega T_L}{2}\right)\sin(\delta\theta) + n_q, \end{aligned} \tag{1}$$

where τ, $\delta\omega$, and $\delta\theta$ denote the mean code phase, carrier frequency, and carrier phase errors, respectively, and $R(\tau)$ is the spreading code autocorrelation function. The variable T_L denotes the coherent integration period and also defines the interval between successive updates of the tracking loop. It is assumed that the coherent integration period is aligned with the data modulation symbol boundaries, such that the variable $d \in \{-1, 1\}$ denotes the data sign, which is constant during correlation interval. Under normal PLL operation, the code phase and carrier frequency are reasonably well tracked by the receiver, such that $R(\tau)\,\mathrm{sinc}(\delta\omega T_L/2) \approx 1$, and so they have a negligible effect on (1). The propagation of the thermal noise to the correlator values is modeled as additive white Gaussian noise (AWGN):

$$n_i, n_q \in \mathcal{N}\left(0, \frac{N_0}{2T_L}\right), \tag{2}$$

where N_0 represents the one-sided thermal noise floor in W/Hz. An estimate of the carrier phase tracking error, $\delta\theta$, is then made by applying a carrier phase discriminator to the values I and Q. This estimation procedure is discussed in more detail in Section 3.

2.2. The Phase-Lock Loop. The standard phase-lock loop is a feedback control loop which tracks the carrier phase using estimates of the carrier phase tracking error. Although all realizable phase error estimators are nonlinear, if the estimate is linearized around zero phase error and normalized such that the noise-free estimate has unity gain, the phase error estimate, denoted by e, can be approximated by [4]

$$e \approx K_D \delta\theta + n_\theta \quad \text{for } -\mathrm{LR} < \delta\theta < \mathrm{LR}, \tag{3}$$

where LR represents the linear region of the discriminator. That is, the phase error estimate is approximately equal to a constant times the true phase error, plus a zero mean, white noise, n_θ. The constant gain, K_D, is referred to as the discriminator gain and depends on the chosen discriminator function and the prevailing signal-to-noise-ratio. The variance of n_θ is also dependent on the phase discriminator used and the received signal-to-noise ratio. The two-sided spectral density of n_θ is denoted here by N_θ. The linear region is defined as the interval $[-\mathrm{LR}, \mathrm{LR}]$, over which this discriminator approximation is valid. The exact details of the linearization of this phase error estimate and the values of the PSD of n^θ for various discriminators will be given in Section 3.

The remainder of the PLL is linear and can be represented by a system of z-domain transfer functions, where the update interval of the system is T_L. Such a linearized loop model is useful as it facilitates the estimation of loop stability and tracking performance. Of particular interest are the transfer functions between the carrier phase, θ, and the carrier phase estimate, $\widehat{\theta}$, between the carrier phase, θ, and the tracking error, $\delta\theta$, and between the thermal noise, n_θ, and the tracking error, $\delta\theta$. These quantities are depicted in a linearized loop model in Figure 1. The transfer functions of interest are given by

$$H_\theta(z) = \frac{\widehat{\Theta}(z)}{\Theta(z)} = \frac{K_D \mathrm{NCO}(z) F(z)}{1 + K_D \mathrm{NCO}(z) F(z)}, \tag{4}$$

$$H_{\delta\theta}(z) = \frac{\Delta\Theta(z)}{\Theta(z)} = 1 - H_\theta(z), \tag{5}$$

$$H_n(z) = \frac{\Delta\Theta(z)}{N_\theta(z)} = \frac{-1}{K_D} H_\theta(z), \tag{6}$$

where uppercase symbols represent the z-transform of the corresponding lowercase time series. The functions $F(z)$ and $\mathrm{NCO}(z)$ represent the z-transform of the loop filter

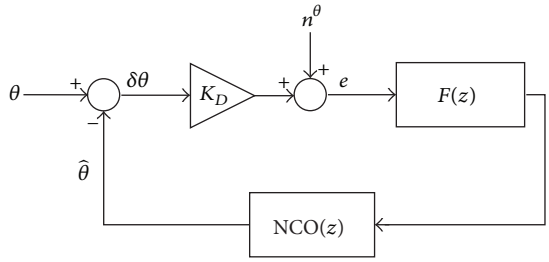

Figure 1: Linearized PLL Model.

and the numerically controlled oscillator, respectively. The numerically controlled oscillator is defined as [4]

$$\mathrm{NCO}(z) = \frac{T_L}{z-1}. \tag{7}$$

Generally, a proportional and integral (PI) controller is used in GNSS PLLs. A generalization of this type of controller takes the form [5]

$$F(z) = \sum_{p=0}^{P} A_p \left(\frac{T_s z}{z-1}\right)^p, \tag{8}$$

where $P+1$ is the order of the resultant closed loop system.

3. Carrier Phase Estimation

As discussed in Section 2.2, the performance of the PLL in the presence of AWGN can be estimated by examining the linear model and the noise performance of the carrier phase discriminator. Four popular carrier phase discriminators are examined here: the four-quadrant arctangent discriminator, the arctangent discriminator, the decision-directed discriminator, and the simple quadrature discriminator. The discriminators are characterized in terms of gain, K_D, and variance, $\sigma^2_{n_\theta}$, where

$$K_D = \left.\frac{\partial \mathrm{E}[e]}{\partial \delta\theta}\right|_{\delta\theta=0}, \tag{9}$$

$$\sigma^2_{n_\theta} = \mathrm{Var}[n_\theta] = \left.\mathrm{Var}[e]\right|_{\delta\theta=0}, \tag{10}$$

and, in Section 3.7, the linear region will also be considered.

In the carrier phase discriminator analysis that follows, it is assumed that the PLL is operating normally, with a mean frequency error of zero and a maximum frequency error that is reasonably small relative to the update interval, such that the phase error accrued over the update interval is less than the linear region of the discriminator, for example.

3.1. Measuring Signal Quality. It will be shown that the performance of the estimators considered in this work varies with the signal-to-noise ratio (SNR) of the correlator values, specifically the coherent SNR, defined as [3, 6]

$$\mathrm{SNR}_c = \left.\frac{\mathrm{E}[I]^2}{\mathrm{Var}[I]}\right|_{\delta\theta=0}. \tag{11}$$

This metric represents the quality of the signals which are applied to the discriminator and is largely the same as the E_b/N_0 metric used in, for example, [7], for characterizing baseband communication systems with the distinction that SNR_c need not, necessarily, correspond to a full bit period. A number of factors influence the value of the SNR_c including the received signal power, the receiver's noise floor, the coherent integration period, the front-end filter, and the quantizer configuration. In an ideal receiver, the value of SNR_c can be related directly to the received carrier-to-noise-density ratio (often denoted C/N_0 or CNR) and the coherent integration time. Similarly, if the losses induced by factors such as front-end filtering and quantization can be modeled as a single loss value, denoted here by L, then the following approximation is valid [3, 8]:

$$\mathrm{SNR}_c \approx \frac{2LCT_L}{N_0}. \tag{12}$$

The advantage of using SNR_c as a signal quality metric, as opposed to C/N_0, for example, is that it reflects all of the signal processing effects applied to the received signal. Therefore, the performance of various discriminators can be related to one signal metric, as opposed to the ensemble of quantities: P, N_0, T_L, L and, perhaps, others. Moreover, as will be shown in Section 5.2, to achieve a specified loop performance it may be necessary to maintain a particular value of SNR_c and so, accordingly a designer may wish to adjust T_L, given a particular C/N_0.

As a numerical example, consider a typical received GPS L1 C/A signal under open sky conditions and a typical consumer grade receiver. The received signal power using a patch antenna will be approximately −160 dBW and the receiver thermal noise floor may be assumed to be −205 dBW/Hz. If the receiver employs a front-end filter with a 2 MHz bandwidth and a one-bit quantizer then the combined receiver processing losses will be approximately 2 dB. Tallying these figures and assuming a coherent integration period of 1 ms, the expected value of SNR_c is 16 dB. Alternatively, if a coherent integration period of 20 ms was assumed then the expected value of SNR_c would be 29 dB. Under weak-signal conditions, however, such as the indoor environment, SNR_c can fall to 0 dB and below.

3.2. The Four-Quadrant Arctangent Discriminator (Atan2). The four-quadrant arctangent discriminator is defined as [8]

$$e_m^{\mathrm{Atan2}} = \arctan 2\left(I_m, Q_m\right), \tag{13}$$

and is a pure-PLL discriminator, appropriate for pilot signals, or when data wipe-off is employed. The mean response of this discriminator to phase error, denoted here by μ_e^{Atan2}, is well known (see, e.g., [8–10]). For high values of SNR_c, μ_e^{Atan2} is relatively linear across a wide range of phase error values and has approximately unity gain. As the value of SNR_c reduces, the gain reduces considerably and the linear region diminishes. Expressions describing the exact mean response of the discriminator and its variance are developed as follows.

If the correlator values are interpreted as a complex pair, $I + jQ$, then the argument, $\arg\{I + jQ\}$, can be shown to be distributed according to the probability density function, $p(\phi)$, defined as [9]

$$p(\phi) = \frac{1}{2\pi} e^{-(\mathrm{SNR}_c/2)} + \frac{1}{2\sqrt{\pi}} e^{-(\mathrm{SNR}_c/2)\sin^2(\phi)} \sqrt{\frac{\mathrm{SNR}_c}{2}} \cdot \cos(\phi) \left(1 + \mathrm{erf}\left(\sqrt{\frac{\mathrm{SNR}_c}{2}} \cos(\phi)\right)\right). \tag{14}$$

Using $p(\phi)$, it can be readily shown that the value of μ_e^{Atan2} is given by

$$\mu_e^{\mathrm{Atan2}} = \int_{-\pi}^{\pi} \arctan 2\left(\cos(\delta\theta + \phi), \sin(\delta\theta + \phi)\right) p(\phi)\, d\phi = \int_{-\pi}^{\pi} \phi p(\phi - \delta\theta)\, d\phi. \tag{15}$$

From (9), taking the first derivative of (15) and setting $\delta\theta = 0$, the discriminator gain is found to be

$$K_D^{\mathrm{Atan2}} = \left.\frac{\partial \mu_e^{\mathrm{Atan2}}}{\partial \delta\theta}\right|_{\delta\theta=0} = \int_{-\pi}^{\pi} \phi p'(\phi)\, d\phi, \tag{16}$$

where $p'(\phi)$ is the first derivative of $p(\phi)$ with respect to ϕ, given by

$$p'(\phi) = \frac{e^{-(\mathrm{SNR}_c/2)}}{4\pi} \sqrt{\mathrm{SNR}_c} \sin(\phi) \cdot \left(\sqrt{2\pi} e^{(1/2)\mathrm{SNR}_c \cos^2(\phi)} \left(\mathrm{SNR}_c \cos^2(\phi) + 1\right) \cdot \left(\mathrm{erf}\left(\frac{\sqrt{\mathrm{SNR}_c}\cos(\phi)}{\sqrt{2}}\right) + 1\right) + 2\sqrt{\mathrm{SNR}_c}\cos(\phi)\right). \tag{17}$$

A plot of K_D versus SNR_c for this discriminator is shown in Figure 2. It is evident that for SNR_c values below approximately 6 dB, the discriminator gain reduces rapidly. This reduction in discriminator gain has implications for the closed loop poles of (4), (5), and (6). This will be discussed further in Section 4.

In a similar fashion to the mean of the four-quadrant arctangent discriminator, the variance of this carrier phase estimate can be found via

$$\mathrm{Var}\left[n^\theta\right] = \int_{-\pi}^{\pi} \arctan 2\left(\cos(\delta\theta + \phi), \sin(\delta\theta + \phi)\right)^2 p(\phi)\, d\phi. \tag{18}$$

This variance estimate, however, is a function of $\delta\theta$. Assuming that the PLL is tracking with an approximately zero mean phase error, it is useful to linearize this estimate around a zero phase error, $\delta\theta = 0$:

$$\mathrm{Var}\left[n^\theta\right] \approx \int_{-\pi}^{\pi} \arctan 2\left(\cos(\phi), \sin(\phi)\right)^2 p(\phi)\, d\phi = \int_{-\pi}^{\pi} \phi^2 p(\phi)\, d\phi. \tag{19}$$

A plot of $\mathrm{Var}[n^\theta]$ for this discriminator is shown in Figure 3. For convenience, approximate solutions to (16) and (19) are provided in the appendix. Unsurprisingly, the discriminator variance changes linearly with SNR_c for high SNR_c values, bearing the approximate relationship: $\mathrm{Var}[n^\theta] \approx 1/\mathrm{SNR}_c$. In this region, (14) is approximately Gaussian. At $\mathrm{SNR}_c \approx 11$ dB the discriminator variance exceeds $1/\mathrm{SNR}_c$ with reducing SNR_c. At this point, (14) has begun to resemble a truncated Gaussian distribution. As SNR_c is further

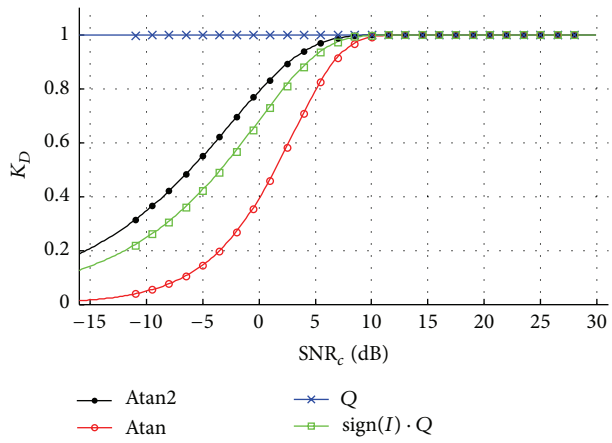

Figure 2: Discriminator gain (K_D) versus SNR_c for the four-quadrant arctangent discriminator (Atan2), the arctangent discriminator (Atan), the quadrature discriminator (Q), and the decision-directed discriminator ($\mathrm{sign}(I) \cdot Q$).

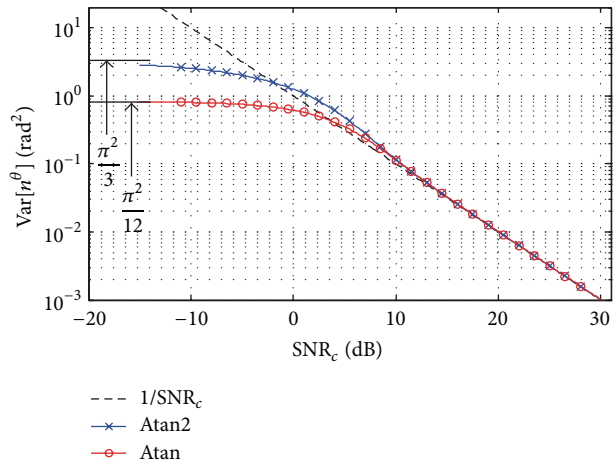

Figure 3: Variance of the carrier phase estimate versus SNR_c, linearized around a zero phase error, for the four-quadrant arctangent discriminator and the arctangent discriminator.

reduced, (14) falls below the $1/\mathrm{SNR}_c$ curve and approaches a uniform distribution over the interval $[-\pi, \pi]$, reaching a maximum variance of $\pi^2/3$. This nonlinear relationship between SNR_c and $\mathrm{Var}[n^\theta]$ has a significant impact on the performance of the PLL under weak-signal conditions and, in conjunction with the discriminator gain effects described earlier, can result in severely degraded tracking performance. These effects must, therefore, be considered in the design of the PLL and will be discussed further in Section 4.

3.3. The Arctangent Discriminator (Atan). The arctangent discriminator is defined as [7, 8, 11]

$$e^{\mathrm{Atan}} = \arctan\left(\frac{Q}{I}\right) \tag{20}$$

and is a Costas discriminator, suitable for use on data-modulated signals. Similar to the four-quadrant arctangent discriminator, for high values of SNR_c, μ_e^{Atan} changes in a relatively linear fashion with changing $\delta\theta$ and has approximately unity gain. As the value of SNR_c reduces, the gain reduces considerably and the linear region diminishes. This occurs at a higher SNR_c value for the arctangent discriminator than for the four-quadrant arctangent discriminator, owing to its smaller linear region (discussed further in Section 3.7).

Similar to Section 3.2, it can be shown that the mean response of the arctangent discriminator, after some simplification, is given by

$$\begin{aligned}\mu_e^{\mathrm{Atan}} &= \int_{-\pi}^{\pi} \arctan\left(\frac{\sin(\delta\theta+\phi)}{\cos(\delta\theta+\phi)}\right) p(\phi)\, d\phi \\ &= \int_0^{\pi} \phi\left(p(\phi-\delta\theta) - p(\phi+\delta\theta)\right) d\phi \\ &\quad - \pi\int_{\pi/2}^{\pi} \left(p(\phi-\delta\theta) - p(\phi+\delta\theta)\right) d\phi,\end{aligned} \tag{21}$$

where the limits of integration have been manipulated such that the arctangent function and its arguments reduce to simple linear combinations of $\delta\theta$, ϕ, and π.

Again, from (9), taking the first derivative of (21) and setting $\delta\theta = 0$, the arctangent discriminator gain, K_D^{Atan}, is found to be

$$\begin{aligned}K_D^{\mathrm{Atan}} &= \left.\frac{\partial \mu_e^{\mathrm{Atan}}}{\partial \delta\theta}\right|_{\delta\theta=0} \\ &= 2\int_0^{\pi} \phi p'(\phi)\, d\phi - 2\pi\int_{\pi/2}^{\pi} p'(\phi)\, d\phi.\end{aligned} \tag{22}$$

Figure 2 depicts the relationship between K_D and SNR_c for this discriminator. For SNR_c values below approximately 10 dB, the discriminator gain reduces rapidly. Although the trend is similar to that of the four-quadrant arctangent discriminator, it occurs at a higher SNR_c value and the reduction in K_D with SNR_c is greater.

Similar to the four-quadrant arctangent discriminator, the variance of this carrier phase estimate, linearized around a zero phase error, can be found via

$$\begin{aligned}&\mathrm{Var}\left[n^\theta\right] \\ &\quad \approx 2\left(\int_0^{\pi} \phi^2 p(\phi)\, d\phi + \pi\int_{\pi/2}^{\pi} (\pi - 2\phi)\, p(\phi)\, d\phi\right).\end{aligned} \tag{23}$$

Figure 3 illustrates this relationship across an appropriate range of SNR_c values. Again, similar to the four-quadrant arctangent discriminator, the discriminator variance changes linearly with SNR_c for high SNR_c values. As SNR_c is reduced, (14) approaches a uniform distribution over the interval $[-\pi/2, \pi/2]$ and reaches a maximum variance of $\pi^2/12$. Once again, approximate solutions to (22) and (23) are provided in the Appendix.

3.4. The Quadrature Discriminator (Q). The quadrature discriminator is defined, as its name suggests, as

$$e^{Q} = Q, \tag{24}$$

which is a pure-PLL discriminator, appropriate for non-data modulated signals. It is also notable both as being the phase detector used in the earliest PLLs; and as being the only discriminator for which the resultant PLL admits tractable nonlinear analysis [12, 13]. This discriminator function is, by far, the simplest form of carrier phase estimator. Owing to its simple definition, the characteristics of this discriminator are quite easily expressed, having a mean value, μ_e^Q, of

$$\mu_e^Q = \mathrm{E}[Q] = d\sqrt{P}\sin(\delta\theta). \tag{25}$$

Unlike the arctangent-based discriminator functions, this phase estimate is not self-normalizing; that is, the estimate is a function of the nominal received signal power. To use this discriminator, even for high SNR_c values (where the arctangent-based discriminators are completely self-normalizing), this phase estimate must be normalized by an estimate of $\sqrt{P}$. The discriminator gain, K_D^Q, is given by

$$K_D^Q = \sqrt{P}, \tag{26}$$

which, unlike the previous three discriminators, is independent of SNR_c. The variance of this carrier phase estimate is given by

$$\mathrm{Var}\left[n^\theta\right] = \mathrm{E}\left[\mathrm{Q}^2\big|_{\delta\theta=0}\right] = \frac{P}{\mathrm{SNR}_c}. \tag{27}$$

Note that when the carrier phase estimate has been correctly normalized by $1/\sqrt{P}$, then the variance of this carrier phase estimate is given by $1/\mathrm{SNR}_c$. This $1/\mathrm{SNR}_c$ curve is illustrated in Figure 3, providing a comparison with the arctangent based discriminators.

3.5. The Decision-Directed Quadrature Discriminator (sign$(I)\cdot Q$). The decision-directed discriminator is defined as [8]:

$$e^{\mathrm{sign}(I)\cdot Q} = \mathrm{sign}(I)\cdot Q. \tag{28}$$

The purpose of the $\text{sign}(I) \cdot Q$ term in this discriminator function is to render it insensitive to data modulation. The Q term provides an estimate of $\delta\theta$ multiplied by the data value d while the $\text{sign}(I) \cdot Q$ term provides an estimate of d. As $d^2 = 1$, this discriminator is (ideally) insensitive to data modulation. The value of $\mu_e^{\text{sign}(I)\cdot Q}$ can be found from

$$\mu_e^{\text{sign}(I)\cdot Q} = \text{E}\left[\text{sign}\,(I) \cdot Q\right], \tag{29}$$

where $\text{E}[\cdot]$ denotes the expectation operator. Since I and Q are statistically independent, then

$$\begin{aligned}\mu_e^{\text{sign}(I)\cdot Q} &= \text{E}\left[\text{sign}\,(I) \cdot Q\right] \text{E}\left[Q\right] \\ &= \text{E}\left[\text{sign}\,(I) \cdot Q\right] \left(d\sqrt{P}\sin\left(\delta\theta\right)\right).\end{aligned} \tag{30}$$

Finding $\text{E}[\text{sign}(I)\cdot Q]$ is equivalent to the estimation of d given the AWGN corrupted sample: $\sqrt{P}\cos(\delta\theta)d + n_i$. It can, thus, be readily shown that [7]

$$\mu_e^{\text{sign}(I)\cdot Q} = \sqrt{P}\,\text{erf}\left(\sqrt{\frac{\text{SNR}_c}{2}}\cos\left(\delta\theta\right)\right)\sin\left(\delta\theta\right). \tag{31}$$

The gain, $K_D^{\text{sign}(I)\cdot Q}$, of this discriminator can be shown, using (9) and (31), to be

$$K_D^{\text{sign}(I)\cdot Q} = \sqrt{P}\,\text{erf}\left(\sqrt{\frac{\text{SNR}_c}{2}}\right). \tag{32}$$

A plot of K_D versus SNR_c is shown in Figure 2.

Unlike the arctangent based discriminators, the variance of the decision-directed discriminator can be readily related to SNR_c. From (10) and (28), we find

$$\begin{aligned}\text{Var}\left[n^\theta\right] &= \text{E}\left[\text{sign}\,(I)^2\, Q^2\big|_{\delta\theta=0}\right] = \text{E}\left[Q^2\big|_{\delta\theta=0}\right] \\ &= \frac{P}{\text{SNR}_c}.\end{aligned} \tag{33}$$

As with the quadrature discriminator, once the carrier phase estimate has been correctly normalized by $1/\sqrt{P}$, then the variance of this carrier phase estimate is given by $1/\text{SNR}_c$, as depicted in Figure 3.

3.6. The Gain-to-Noise Ratio (GNR). Sections 4.3 and 5 will illustrate that the performance of the tracking loop can be related, amongst other things, to the gain and variance of the discriminator. In fact, it will be shown that, under steady-state conditions, it is directly related to the ratio of the square of the gain to the variance. It is useful, therefore, to consider this ratio as a metric by which the tracking capability of each discriminator can be compared. This metric, termed the gain-to-noise ratio and denoted by GNR, is defined as

$$\text{GNR} = \frac{K_D^2}{\text{Var}\left[n^\theta\right]}. \tag{34}$$

A plot of GNR for each of the four discriminators is shown in Figure 4. As can be expected from the analysis presented in Section 3, under high SNR_c conditions ($\text{SNR}_c > 12$ dB, e.g.), the GNR for each discriminator is similar. The reason for this is that for these high SNR_c values $K_D \approx 1$ and $\text{Var}[n^\theta] \approx 1/\text{SNR}_c$ for each of the four discriminators. For reduced SNR_c conditions, however, the unique relationship between K_D, $\text{Var}[n^\theta]$, and SNR_c for each discriminator becomes evident. As the gain and variance characteristics of each discriminator are different, the GNR curves diverge as SNR_c is reduced. Because the tracking capability of the PLL can be directly related to the GNR (as will be shown in Section 4.3), it provides insight into the relative tracking performance of each discriminator. Interestingly this metric also provides some insight into the relative benefits of a pilot signal, as it is clear that the GNR of the pure-PLL discriminators is noticeably higher than that of the Costas discriminators for SNR_c values below approximately 5 dB, as will be discussed further in Section 5.4.

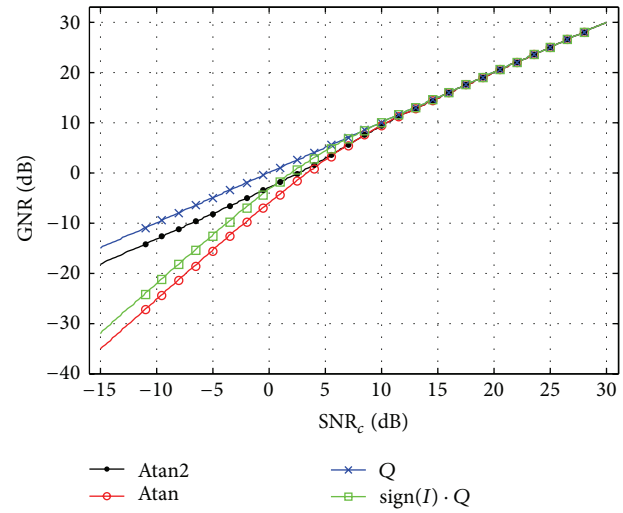

Figure 4: GNR versus SNR_c for the four-quadrant arctangent discriminator, the arctangent discriminator, decision-directed discriminator, and the quadrature discriminator.

While the GNR can provide valuable insight into the operation of the PLL in its linear region, it does not completely characterize the discriminator's influence on closed loop operation, as will be discussed next.

3.7. The Discriminator Linear Region. The linearized discriminator model employed in previous sections is an optimistic performance model and, generally, is only accurate for a limited range of $\delta\theta$. This range is termed the linear region and is finite for all discriminators. Indeed, it is ultimately limited to the range $[-\pi, \pi]$, owing to the periodic nature of the sinusoid. As has been shown in the previous sections, the values of K_D and μ_e are dependent on the discriminator function, and, with the exception of the quadrature discriminator, are also dependent on SNR_c.

In general, the linear region is symmetric around the origin and so it can be defined by the single scalar LR such that the linear region is the interval $[-\text{LR}, \text{LR}]$. LR is defined

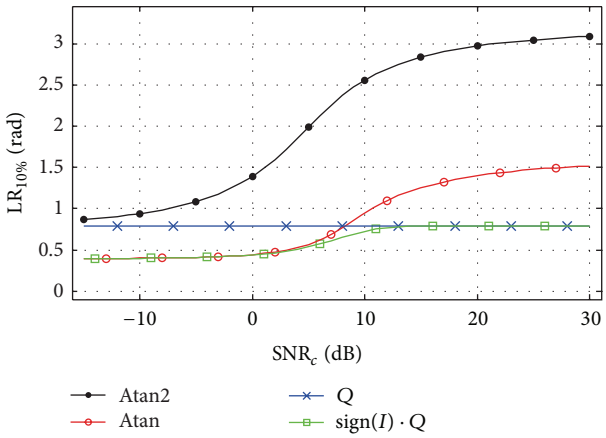

FIGURE 5: $LR_{10\%}$ versus SNR_c for the four-quadrant arctangent discriminator (Atan2), the arctangent discriminator (Atan), decision-directed discriminator ($\text{sign}(I) \cdot Q$), and the quadrature discriminator (Q).

as the value of $\delta\theta$ at which the true value of μ_e and the approximation $\mu_e \approx K_D\delta\theta$ differ by a certain percentage. The percentage is chosen arbitrarily, often depending on the application, but typical values are 5% and 10%. Specifically, LR for an x% linear region, denoted $LR_{x\%}$, is defined as

$$LR_{x\%} = \left\{\delta\theta \in \mathbb{R} : \frac{K_D\delta\theta}{\mu_e} = \left(1 - \frac{x}{100}\right),\ \delta\theta > 0\right\}, \quad (35)$$

where the notation $A = \{B \in C : D\}$ can be interpreted as A equals values of B in the set C such that condition D is satisfied.

It is, thus, the intersection of the mean discriminator curve and the line $(x/100)K_D\delta\theta$ that defines the linear region.

A plot of $LR_{10\%}$ versus SNR_c is shown in Figure 5. Examining the pure-PLL discriminators, it can be seen that the four-quadrant arctangent discriminator has a significantly larger linear region than the quadrature discriminator over the entire SNR_c range of interest. For the Costas case, the arctangent discriminator has a significantly larger linear region than the decision-directed discriminator, for high SNR_c values. For SNR_c values below approximately 7 dB, however, the linear region of both discriminators converge. The implications of the specific LR values and their dependence on SNR_c will be discussed further in Section 5.

4. Closed Loop Operation

This section examines the closed loop operation of the PLL, specifically investigating the relationship between the discriminator gain and variance and their SNR_c-dependence on the closed loop transient and steady-state behavior. The relationship between the tracking bandwidth and the SNR_c-dependent discriminator gain is examined theoretically and the resultant influence on the transient response is illustrated via simulated phase step-tests. In terms of steady-state performance, the significance of the GNR metric as a means of predicting thermal noise induced tracking error is examined.

4.1. Tracking Bandwidth. The design of PLL loop filters is often a delicate balance between a sufficiently fast loop to cope with satellite-to-user dynamics, and a sufficiently slow loop to resist thermal noise induced tracking error. It is crucial, therefore, that a designer has control over the exact placement of the loop poles. In general, direct specification of the closed loop poles is not intuitive and, so, the pole placement is often specified in terms of damping coefficient and equivalent bandwidth (second-order-dominant systems are generally parametrized in terms of the system damping coefficient, ζ, and natural frequency, ω_n, each of which a uniquely observable effect in the time-domain [5]; when considering the system in terms pole-zero placement, however, it is more convenient to reparametrize the system in terms of the dominant poles, given by $-\beta(1 \pm \eta)$ which can be related via $\beta = \omega_n\zeta$ and $\eta = \sqrt{1 - \zeta^{-2}}$.)

The effective *two-sided* rectangular bandwidth of the closed loop transfer function, denoted here by B_θ, is defined as

$$B_\theta = \frac{1}{2\pi T_L}\int_{-\pi}^{\pi} \left|H_\theta\left(e^{j\omega}\right)\right|^2 d\omega. \quad (36)$$

Generally, $|H_\theta(e^{j\omega})|^2$ will be low-pass, with a relatively smooth pass-band. B_θ, therefore, is indicative of the speed at which the PLL will settle.

It is important to note the presence of K_D in both the numerator and denominator of $H_\theta(z)$ in (4). As has been shown in Section 3, K_D is dependent on the prevailing SNR_c. For low SNR_c values, the value of K_D is less than unity and, therefore, the effective bandwidth of the PLL will be less than its design value. As will be shown in Sections 4.2 and 5.1, this can have a significant impact on the overall loop performance.

In light of this effect, it is convenient to denote the high-SNR_c value (or the design value) of B_θ by B_θ^{Design} and to define it as

$$B_\theta^{\text{Design}} = B_\theta\big|_{K_D=1}. \quad (37)$$

Examining $H_\theta(z)$ once again, it is clear that the denominator can be rendered independent of K_D by scaling $F(z)$ or, more specifically, the gains, A_p, by a factor $1/K_D$. To implement this gain-compensation the receiver must estimate the prevailing value of SNR_c and calculate the value of K_D corresponding to this value and the particular discriminator employed. This approach maintains the value of B_θ at the prescribed value B_θ^{Design}, regardless of the prevailing SNR_c. Note that although this gain-compensation modifies the loop filter gains as the prevailing signal strength changes, it is not an adaptive loop; it merely corrects for gain degradation in order to maintain a constant loop bandwidth. The effects of K_D and benefits of this gain-compensation are explored next.

4.2. Transient Response. This section examines the transient response of a second-order PLL employing an arctangent discriminator and a loop update rate of $T_L = 1$ ms under both high- and low-SNR_c conditions. The loop filter, detailed in Table 1, effects a critically damped system, $\eta = 0$, with

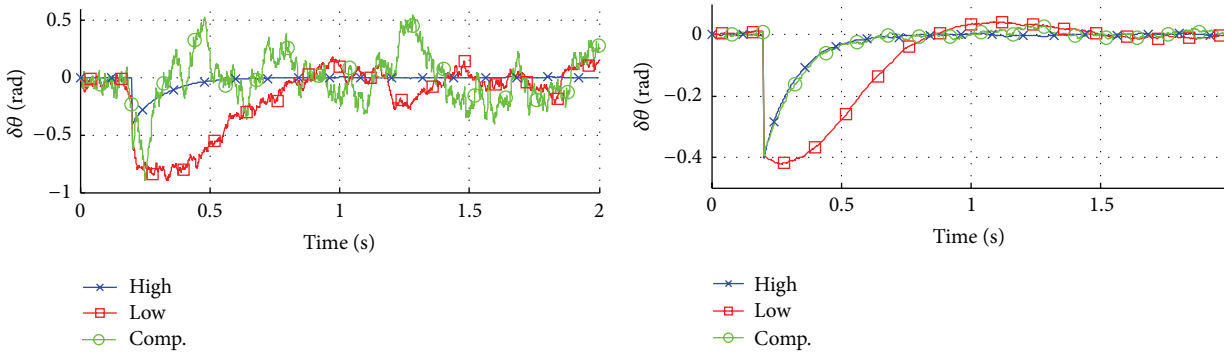

(a) One instance of the PLL response

(b) The mean response calculated over 500 trials

FIGURE 6: The response of the PLL to phase and frequency steps of −0.4 rad and -1.2π rad/s, respectively.

TABLE 1: PLL design parameters for transient response experiment.

	High	Low	Comp.
T_L (s)	0.001	0.001	0.001
K_D	1.0	0.4	0.4
$\{A_0, A_1\}$	{16.35, 65.10}	{16.35, 65.10}	{41.46, 165.14}
z_0	0.9912	$0.996 - 0.00398i$	0.9913
z_1	0.9927	$0.996 + 0.00398i$	0.9927
β	8.06	4.01	8.06
η	0.0	$-0.996i$	0.0
ζ	1.0	0.71	1.0
B_θ (Hz)	10.0	5.22	10.0

a tracking bandwidth of $B_\theta = 10$ Hz. The system was excited by a simultaneous step in phase of -0.12π rad and a step in frequency of -1.2π rad/s. An example of a simulated response of the PLL to this excitation, for a signal received at an SNR_c of 23 dB, is plotted in Figure 6(a) and labeled "High." As can be seen, the PLL exhibits a smooth, critically damped response which settles to within 5% of its peak value within 0.5 s.

To illustrate the impact of the SNR_c-dependent K_D on the transient response of the PLL, this simulation was repeated under "Low"-SNR_c conditions. The particular case of SNR_c of 0 dB was chosen as it corresponds to $K_D = 0.4$ for the arctangent discriminator (see Figure 2). An example of the PLL response in this case is shown in Figure 6(a) and labeled "Low." It is evident, apart from the increased noise, that the response of the PLL has become slower and more oscillatory.

This transient was simulated a total of 500 times, for both the high-SNR_c and the low-SNR_c cases and the average response was calculated and is presented in Figure 6(b), labeled "High" and "Low," respectively. Indeed, it can be seen that the reduction in SNR_c has induced a slower and underdamped response. Given $K_D = 0.4$, this has been calculated to be $\zeta = 0.71$.

Using (36), B_θ was calculated for both the high-SNR_c case and the low-SNR_c cases to be 10 Hz and 5.28 Hz, respectively. It is clear that the value of B_θ is significantly reduced by the reduction in K_D, an observation which agrees with Figure 6(b), in the sense that reduced B_θ results in an increased mean time to settle.

To eliminate this effect, the gain compensation discussed in Section 4.1 was applied to the PLL and the low-SNR_c scenario of 0 dB was reprocessed. The parameters of the compensated loop are presented in Table 1, in the column labeled "Comp.". An example of the K_D compensated loop response is shown in Figure 6(a). Again, the mean value of this response is estimated over 500 trials and is plotted in Figure 6(b). It is clear that the mean response is restored to that of the high-SNR_c case. Restoration of the PLL transient performance does, unfortunately, come at a price. It can be seen in Figure 6(a) that the K_D-compensated loop response exhibits significantly more thermal noise induced tracking error. This has implications for the steady-state operation of the PLL and is discussed next.

4.3. Tracking Error/Jitter. Following the transient response of the PLL, once the signal parameters (phase, Doppler, and higher order effects) have been estimated, the PLL settles and tracks the carrier phase. This so-called steady-state performance is, typically, dominated by thermal noise. The performance of the PLL in the presence of thermal noise can be measured in terms of the steady-state tracking error variance or tracking jitter, denoted here by $\sigma^2_{\delta\theta}$. In the case of the PLL, the noise which corrupts the estimate $\widehat{\theta}$ of the carrier phase θ is n_θ and has propagated through the discriminator. Similar to the thermal noise floor, N_0, it is convenient to consider an equivalent noise floor for the tracking error estimate, e. Denoted here by N_θ, the noise floor of the phase error estimate, in rad^2/Hz, is defined as

$$N_\theta = T_L \,\text{Var}\left[n^\theta\right]. \tag{38}$$

Note that, unlike N_0, N_θ is defined as a two-sided PSD. Given the transfer function $H_n(z)$ and (38), the tracking error variance can be estimated as

$$\sigma^2_{\delta\theta} = \frac{N_\theta}{2\pi T_L} \int_{-\pi}^{\pi} \left|H_n\left(e^{j\omega}\right)\right|^2 d\omega. \tag{39}$$

Although N_θ can be well approximated by $N_0/2$ for high values of SNR_c, for lower values of SNR_c their values

diverge and N_0 alone cannot be used to predict closed loop performance.

Using (39), the impact of K_D on the noise performance of the PLL can be examined. As discussed in Section 4.2, it is necessary to compensate for the SNR_c-induced reduction in K_D by increasing the filter gains, A_p, by a factor $1/K_D$. Using such gain-compensation, from (6), $\sigma^2_{\delta\theta}$ is given by

$$\sigma^2_{\delta\theta} = \frac{\mathrm{Var}\left[n^\theta\right]}{K_D^2} B_\theta \Bigg|_{A_p \to A_p/K_D} = \frac{\mathrm{Var}\left[n^\theta\right]}{K_D^2} B_\theta^{\mathrm{Design}} = B_\theta^{\mathrm{Design}} \mathrm{GNR}^{-1}. \tag{40}$$

This result implies that, given perfect K_D compensation, $\sigma^2_{\delta\theta}$ is equal to a constant term, $B_\theta^{\mathrm{Design}}$, divided by the ratio $K_D^2/\mathrm{Var}[n^\theta]$. Although the ratio $\mathrm{Var}[n^\theta]/K_D^2$ appears in (40), its reciprocal is chosen as the definition of the GNR; this is done so that GNR conforms with metrics such as SNR_c, SNR_{nc}, and C/N_0, where the numerator pertains to the signal and the denominator pertains to the noise; also, this definition of GNR can be used as a measure of usefulness; the higher the GNR, the more useful the discriminator estimate. As the name suggests, the constant term, $B_\theta^{\mathrm{Design}}$, is chosen by the designer. The ratio, $K_D^2/\mathrm{Var}[n^\theta]$, is related to SNR_c via a function which is particular to each discriminator, defined earlier as GNR.

To illustrate the usefulness of the GNR in predicting the relative closed loop performance of various discriminators in the presence of thermal noise, the tracking error variance of a simulated PLL was measured for each of the four discriminators, across a range of SNR_c conditions. The loop filter configuration of Table 1 was used and perfect K_D compensation was applied to the loop filter gains for each case. A total of 29 SNR_c conditions were simulated, ranging from −5 dB to 23 dB which corresponds to a C/N_0 range of 22 to 50 dB Hz and $T_L = 1$ ms, for each of the four discriminators. The results of the Monte-Carlo simulations are presented in Figure 7. Using (40), the theoretically predicted variance was calculated and is also plotted in Figure 7, exhibiting good agreement with the simulation results. For SNR_c values below approximately 0 dB, the simulation results for the arctangent and decision-directed discriminator have been omitted. In these cases, the PLL has lost lock and the resulting measurements of tracking error variance are meaningless.

Examining the relative performance of the four discriminators in Figure 7, we see that, for high SNR_c values, all four discriminators perform equally well. As the SNR_c is reduced, however, the individual characteristics of each discriminator influence the performance. These trends compare well with those observed in Figure 4. In fact, from (40), the relative relationship is identical as the curves of Figure 7 are simply the reciprocal of the curves of Figure 4 multiplied by the constant $B_\theta^{\mathrm{Design}}$. It is noticeable that, for $\mathrm{SNR}_c < 8$ dB, both of the Costas discriminators perform more poorly than the pure-PLL discriminators. This is to be expected and is the unavoidable cost of achieving insensitivity to data modulation.

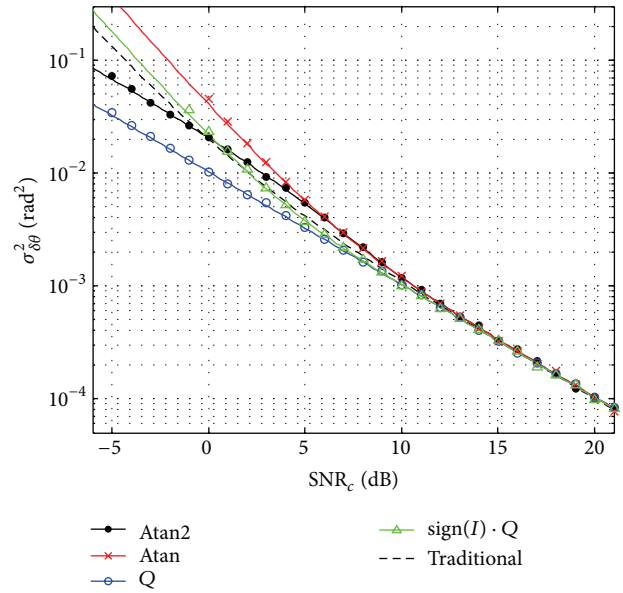

Figure 7: $\sigma^2_{\delta\theta}$ versus SNR_c for $B_\theta^{\mathrm{Design}} = 10$ Hz and each of four discriminators for both simulated (markers) and theoretical (solid) results and traditional theoretical model (dashed).

It is worth mentioning how the tracking jitter curves presented here compare with the traditional theory, which offers two different equations, one representing the class of pure-PLL discriminators, both the quadrature and four-quadrant arctangent, and another representing the Costas discriminators, including the decision-directed quadrature discriminator and the arc tangent discriminator.

Included in Figure 7, for comparison purposes, is a plot of the traditional theoretical performance estimate, representing the general class of Costas discriminators [8, 16]. While this offers a reasonable fit for high SNR_c values and aligns within 15% of the measured performance of the decision-directed quadrature discriminator, it diverges from the measured performance of the arctangent discriminator with reducing SNR_c, being in error by over 50% by an SNR_c of 4 dB, and further diverging below this value. Interestingly, the traditional theory describing the performance of the class pure-PLL discriminators coincides exactly with that presented here for the quadrature discriminator. However, it offers a very poor fit to the performance of the four-quadrant arctangent discriminator being in error by 50% by an SNR_c of 7 dB.

It is reasonable, therefore, to conclude that a comparison of the relative closed loop tracking performance of PLLs which employ the same loop filter, but different discriminators, can be inferred directly by simply examining the relative GNR of the discriminators. That is, the relative linear closed loop performance of two PLLs, for any loop configuration, can be inferred by simply examining the open loop behavior of their respective discriminators. This will be discussed further in Section 5.2 and the usefulness of the GNR in choosing a particular discriminator for a given application will be discussed.

5. Applications to Receiver Design

This section discusses applications of the theory developed in the previous section to GNSS receivers in the context of initial design choices and run-time receiver tuning. Firstly, the importance of acknowledging the dependence of the discriminator gain on the prevailing signal conditions and the benefits of compensating for this gain are considered by examining real GPS L1 C/A for a pedestrian navigation scenario. Secondly, the problem of choosing an appropriate discriminator, given a receiver configuration and received signal strength, is addressed by utilizing the GNR and the linear region metrics. Finally, and once again employing these two metrics, the issue of optimal combining of carrier phase error estimates in data-pilot systems is examined using the Galileo E1 B/C signals as a case study.

5.1. Maintaining the Design Loop Bandwidth. The impact of the discriminator gain on the performance of a GPS L1 C/A tracking loop is examined here in the context of pedestrian navigation. The experiment encompassed a range of SNR_c conditions and considered both tracking loops which employ K_D gain-compensation and those which do not. Results show that loops which compensate for K_D exhibit significantly improved cycle-slip performance.

A set of IF data was collected using a GPS-1A front-end and an Antcom antenna [17, 18] which logged two-bit IF samples at a rate of 16 Ms/s and employed a 2 MHz front end filter. The antenna and receiver were mounted on a rigid body and carried in the pedestrian's hand. Under open-sky conditions, the subject initially stood for one minute and subsequently traversed a 150 m east-west path, repeatedly, at a steady walk for a period of four minutes. The antenna was maintained approximately level for the duration of the experiment and, being hand-held, the antenna, oscillator, and receiver experienced the typical dynamics of a pedestrian including gross velocity of each traversal and the transient, step-induced accelerations.

One particular satellite, PRN 17, was observed at azimuth and elevation of approximately 80° and 78°, respectively, and a received C/N_0 of approximately 46 dB Hz. This signal was tracked using a typical tracking configuration, consisting of a second-order 20 Hz PLL using an arctangent discriminator, defined by (20), and a 0.5 Hz second-order delay-lock loop (DLL). Both tracking loops used a 1 ms update rate. A second-order non-carrier-aided DLL was chosen to ensure that carrier-phase tracking errors, induced by the oscillator and pedestrian dynamics, were not propagated to the code tracking loop.

The observed carrier Doppler is presented in Figure 8. The first sixty seconds represent the stationary part of this experiment where only the satellite-induced Doppler is evident. The remainder of the data represents walking dynamics where both the satellite- and pedestrian-induced gross velocities contribute the observed Doppler. In addition to the gross Doppler, the transient accelerations associated with walking have induced quasisinusoidal perturbations to the observed Doppler via the so-called g-sensitivity of the oscillator [19]. Typically, a temperature compensated crystal oscillator (TCXO) used for hand-held GNSS applications will exhibit a g-sensitivity of the order of 1.5 to 2.5 ppb/g, while specialized low g-sensitivity oscillators are in the range of 0.35 to 0.5 ppb/g (see, e.g., [15]). The dynamics of a walking stride can be expected to induce acceleration peaks and troughs of approximately 8.0 and −6.0 m/s, respectively [21]. Given these values, the Doppler perturbations visible in Figure 8 appear consistent with what would be expected for a low-power low-cost device.

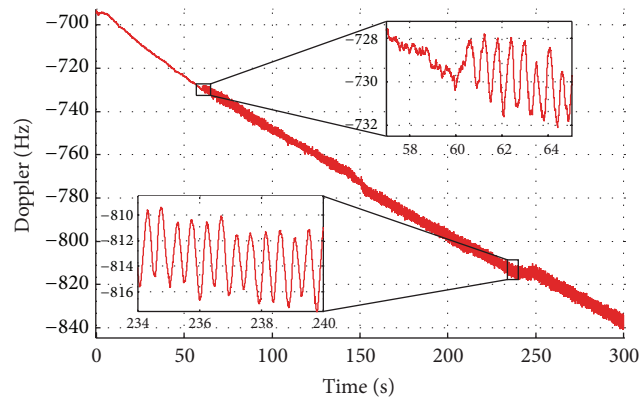

Figure 8: The observed Doppler on PRN 17 during the pedestrian data collection. Highlighted are the transition from standing to walking, at approximately 60 seconds, and the most harsh Doppler perturbations induced by the pedestrian dynamics, at approximately 235 seconds.

To observe the behavior of the carrier tracking loops under weak-signal conditions, the IF data was attenuated prior to reprocessing. This attenuation was achieved by adding white Gaussian noise directly to the IF samples such that the noise power spectral density in the vicinity of the carrier frequency was increased by the required amount. The tracking loops were initialized using the carrier frequency, carrier phase, and code phase estimates gained from the reference, unattenuated trial. An estimate of the tracking performance was then made by comparing the carrier phase estimate of the PLL during the attenuated trial to that of the reference trial. This experiment was then repeated for a selection of signal attenuation values for both the gain-compensated and non-gain-compensated PLLs. Specifically, the data was processed for each of 9, 12, 15, and 18 dB of attenuation, which corresponds to average SNR_c values of 12.1, 9.1, 6.1, and 3.1 dB, respectively. These values of attenuation were chosen to cover an interesting range of discriminator behavior, including the transition from unity gain to progressively reducing gain, including the onset of discriminator variance saturation and including the steepest region of contraction of the linear region. In this way, it is expected that the performance should degrade rapidly with increasing attenuation level and that the application of gain-compensation should improve, to some extent, the performance.

An estimate of the carrier discriminator gain was produced within the gain-compensated PLLs by applying a standard SNR_c estimator to the correlator values, I and Q [8], and using this SNR_c estimate in conjunction with the equations

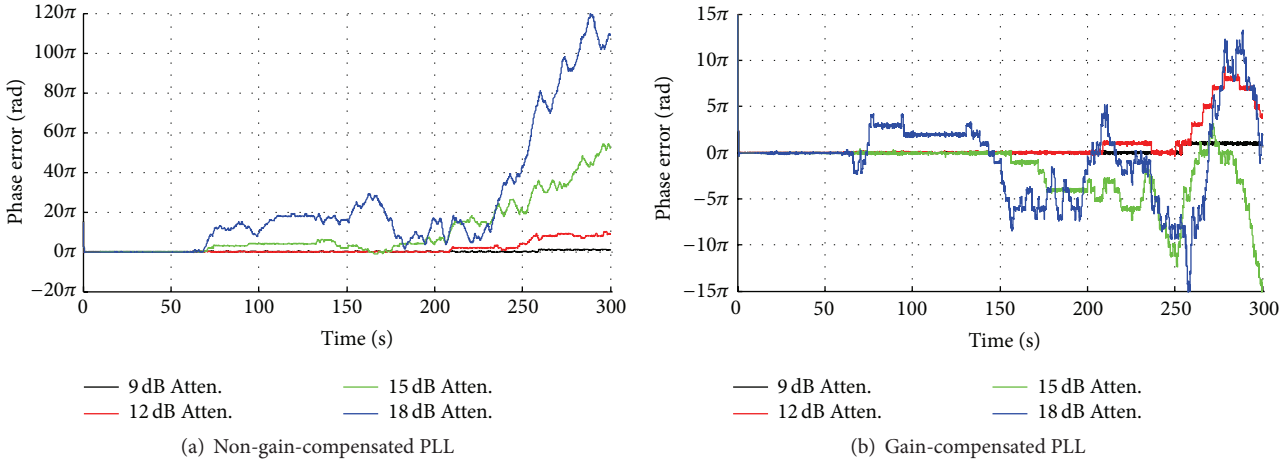

(a) Non-gain-compensated PLL

(b) Gain-compensated PLL

FIGURE 9: The phase error of the PLL over time for a selection of signal attenuations values of 9, 12, 15, and 18 dB for both PLLs which do not apply gain-compensation (a) and those which do (b).

provided in the appendix. Details of the accuracy of SNR_c estimation and the relative sensitivity of the PLL tuning are discussed further in Section 5.3. Figures 9(a) and 9(b) show the measured phase error for the non-gain-compensating and the gain-compensating loops. Apart from the obvious observations that cycle-slips only occur once the pedestrian has begun to walk (from 60 seconds onwards), and that cycle-slips are more frequent in the more highly attenuated trials, there are some more interesting features of these results.

Firstly, it is clear that the gain-compensating loop exhibits significantly less slips than the non-gain-compensating loop. This is due to the fact that the gain reduction induces a slower response to changes in the received phase, thereby resulting in a failure to adequately track the phase trajectory. This observation is supported by the results presented in Table 2, which shows the number of measured half-cycle-slips for five visible satellites. The tabulated data is arranged as follows: each row represents a single satellite, the first and second columns of each row are the PRN and the C/N_0 at which the signal was observed prior to attenuation. The remaining columns represent the total number of half-cycle-slips observed during the attenuated trial, with a pair of numbers per attenuation value. The leftmost number represents the number of half-cycle-slips observed on the nongain compensated PLL, while the rightmost, italic number represents the cycle-slips observed by a PLL implementing live gain-compensation. Secondly, considering the C/N_0 and attenuation numbers from Table 2, it is evident that the benefits of gain-compensation are most pronounced within an SNR_c range of 5.0 to 12.0 dB, which corresponds to the point at which the linear region of the discriminator begins to contract. In this range, the PLL is most sensitive to large sustained phase errors, resulting from a low discriminator gain, as it drastically increases the probability of a cycle-slip. For SNR_c values below this range, the increased noise present on the phase error estimate, the GNR of the discriminator as significantly reduced, and the contribution of thermal noise error becomes significant. Ultimately, of course, the design bandwidth of the PLL ought to be reduced to effect a more reasonable tradeoff between dynamic and thermal noise errors.

TABLE 2: Cycle-slip statistics for attenuated walking trials.

PRN	C/N_0 (dB Hz)	Attenuation (dB)							
		9.0		12.0		15.0		18.0	
4	42.7	2	*1*	29	*8*	211	*104*	—	—
9	46.0	0	*0*	20	*6*	145	*40*	439	*183*
17	47.4	1	*1*	27	*18*	202	*77*	443	*227*
27	45.8	0	*2*	46	*18*	202	*66*	470	*216*
28	44.6	3	*1*	32	*9*	183	*82*	411	*369*

Although this particular experiment only investigates the arctangent discriminator, the general results support the observations made in Section 4.2 and suggest that a similar trend may be observed in the case of other discriminators which exhibit low SNR_c induced gain-degradation. It should be noted that gain compensation is employed exclusively here; however, in some cases, the problem of gain degradation can be circumvented by simply increasing the coherent integration, thereby increasing SNR_c and placing the discriminator in its unity-gain region. Unfortunately, this approach is not always possible. Firstly the integration period may be limited by data modulation and, secondly, either local oscillator instability and/or excessive user dynamics can induce sufficiently rapid phase variations as to necessitate a high loop update rate to maintain phase-lock; that is, net phase dynamics may limit the integration period. Under these circumstances, gain compensation can prove useful.

It is worth commenting on the difference between gain-compensation, as implemented in this experiment, and traditional gain-scheduling or adaptive filtering. The process of gain compensation maintains a constant tracking bandwidth, B_θ, across a range of SNR_c conditions. In contrast, gain-scheduling prescribes a particular loop filter which is deemed appropriate for the prevailing signal conditions and

an adaptive filter will modify its filter parameters in response to features of the received signal (SNR_c, e.g.) [20]. Gain-compensation does not adapt the PLL bandwidth, it ensures that it remains constant and equal to the design bandwidth, B_θ^{Design}. With this in mind, it is clear that the effective implementation of a gain-scheduled or adaptive PLL must consider the effect of SNR_c on the discriminator and employ appropriate gain-compensation.

5.2. Choosing a Discriminator for Linear Operation. Section 4.3 has shown that the closed loop tracking jitter observed in a PLL can be related directly to the GNR and the PLL bandwidth. By examining the relative GNR values of different discriminators, in Figure 4, in conjunction with their linear regions, in Figure 5, it is possible to choose a discriminator which will minimize $\sigma_{\delta\theta}^2$ for a given loop filter choice.

The first, perhaps obvious, conclusion that can be drawn from these figures is that the better of the two pure-PLL discriminators always outperforms the better of the two Costas discriminators, in terms of GNR and linear region. Therefore, if the received signal is not data modulated, or if the modulation is known, then one of the pure-PLL discriminators will always yield the better steady-state tracking performance. A Costas discriminator should only be used when necessitated by the presence of unknown data-modulation. Thus, the choice of discriminator should then be considered for two different discriminator classes, namely, pure-PLL or Costas.

For the pure-PLL discriminators, under high SNR_c conditions (>11 dB), the four-quadrant arctangent discriminator incurs less than a 10% performance degradation, when compared with the quadrature discriminator, yet it exhibits a significantly larger linear region. The four-quadrant arctangent discriminator should, therefore, be used in this region as it provides more robustness than the quadrature discriminator, being capable of absorbing larger phase transients while maintaining linear operation.

In the region $-3\,\text{dB} < SNR_c < 11\,\text{dB}$, the optimum choice of discriminator may be dependent on the application, the quadrature discriminator significantly outperforms the four-quadrant arctangent discriminator in terms of tracking error but has a notably narrower linear region. For applications where low tracking error is the main priority, the quadrature discriminator should be used whereas, if resilience to signal dynamics is desired, a designer may wish to avail of the larger linear region of the four-quadrant arctangent discriminator. For very low SNR_c values (<−3 dB), the linear regions of both discriminators are similar, yet the quadrature discriminator provides approximately 3 dB less tracking error variance and should, therefore, be used.

Unlike the pure-PLL discriminators, the choice of discriminator is simpler for the Costas case. At $SNR_c \approx 9\,\text{dB}$, the linear regions of the arctangent discriminator and the decision-directed discriminator begin to converge. Also, for reducing SNR_c values around this point, the GNR of the decision-directed discriminator begins to significantly outperform the arctangent discriminator. Thus, for SNR_c values above approximately 9 dB, the arctangent discriminator should be used while, for SNR_c values below this point, the decision-directed discriminator should be employed.

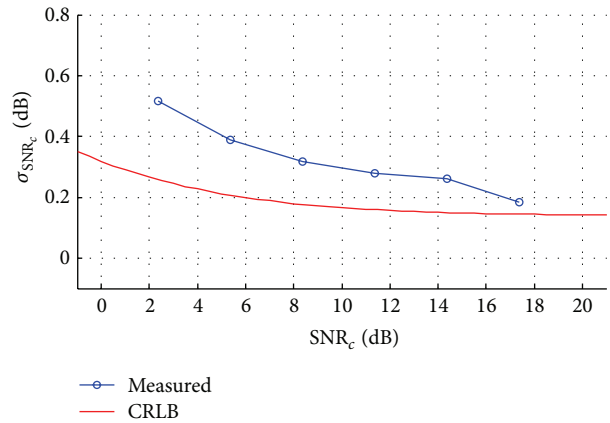

Figure 10: The measured standard deviation the receivers estimate of SNR_c for the walking tests described in Section 5.1, compared to the Cramér-Rao Lower Bound.

Although these conclusions have been drawn from inspection of Figures 4 and 5, they can also be inferred from inspection of the Monte-Carlo simulation results presented in Section 4.3.

5.3. A Note on SNR_c Estimation. As the configuration and tuning of the PLL described here are based on the premise that the prevailing SNR_c is reasonably well known, it is worth briefly commenting on the sensitivity of the PLL tuning to errors in the estimate of SNR_c. Here, the experiment described in Section 5.1 is taken as an example. In this case, a run-time estimate of SNR_c was generated using the well-known estimator described in [8] and further smoothed by a 1 second moving-average filter. Ideally, the choice of smoothing applied to the C/N_0 estimate should reflect a reasonable trade-off between noise-rejection and the speed of response to C/N_0 changes; however, this empirically derived configuration has proven effective.

Recall that the IF data was digitally attenuated by a precise factor for each trial. A reference measurement of the original unattenuated SNR_c was taken, and being a very high value of approximately 22 dB, it was considered to be an error-free estimate. Then, for each attenuated trial, the difference between this reference SNR_c value and the run-time SNR_c estimate, minus the applied attenuation, was recorded. This represented the error in the run-time SNR_c estimate. A plot of the measured standard deviation of the error is shown in Figure 10, along with the Cramér-Rao Lower Bound standard deviation for non-data-aided BPSK SNR_c estimation [22, 23].

In terms of sensitivity to errors in the estimate of SNR_c, the expressions for discriminator gain, K_D, and tracking bandwidth, B_θ, presented in the appendix, can be used to explore the how accurately the loop bandwidth can be restored under low-SNR_c conditions. Assuming a second-order PLL and the arctangent discriminator, and using (A.3) and (A.5), the envelope of B_θ was computed for $SNR_c + \Delta SNR_c$, using the the CRLB shown in Figure 10 as a reference. These envelopes are shown in Figure 11 along with the tracking bandwidth for the cases of perfect compensation

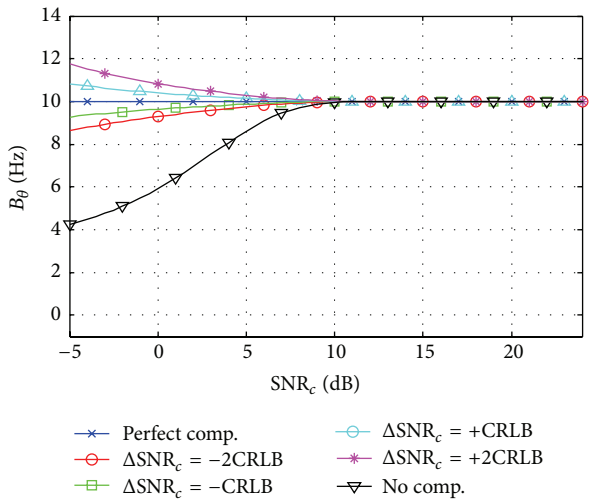

FIGURE 11: Tracking bandwidth, B_θ versus SNR$_c$ when gain compensation is applied given an erroneous estimate of the prevailing signal-to-noise ratio. Note that the magnitude of the error, ΔSNR$_c$, is also a function of SNR$_c$.

and of no compensation. Interestingly, even for very weak-signal conditions, down to an SNR$_c$ of 0 dB, the bandwidth can typically be restored to within one Hertz of its design value. For lower SNR$_c$ values, however, the error becomes noticeable, suggesting that more averaging should be applied in the signal-to-noise ratio estimator, in order to provide a less noisy estimate.

5.4. Choosing a Discriminator for Data/Pilot Tracking. This section examines the problem of carrier tracking for a data-pilot signal structure, specifically, the Galileo E1 B/C signal is taken as an example. Of particular interest is the scenario when the receiver has synchronized with the secondary code on the pilot component of the signal and is capable of combining both a Costas (E1-B) and a pure-PLL (E1-C) estimate of the carrier phase error. The benefits of using the GNR and linear region analysis presented in Section 3, when choosing weights for estimate combining, will be illustrated and some further considerations will be discussed.

A five-minute IF data-set was collected using a roof-mounted antenna during which time the Galileo Prototype Flight Model (PFM) satellite was broadcasting on PRN 11. A complex sample rate of 20 MHz was used and data was collected with a fourteen-bit quantizer resolution. The received signal was observed at a C/N_0 of approximately 47 dB Hz.

Reference carrier phase and frequency trajectories were extracted from this dataset for use in the following experiments. This was done by processing the data with a standard pilot-only tracking architecture, comprising a 4 Hz PLL bandwidth operating with an update rate of 20 ms, combined with a 0.1 Hz PLL-assisted DLL. As the antenna was stationary and the reference oscillator was particularly stable, the use of a low-bandwidth PLL and long coherent integration period ensured that these reference measurements were of high accuracy. An attenuated copy of this data was then processed using different and pilot-only or data/pilot architectures, using a more typical PLL design. The difference between the estimated carrier phase and frequency for these architectures and that of the reference was used as an indication of relative performance.

When processing a data/pilot signal, a PLL can either produce phase estimates using the pilot signal alone, or combine estimates from both the data and the pilot signal (see, e.g., [10, 14]). When two estimates are combined, they can be weighted such that the tracking jitter is minimized. The combined estimate and the associated tracking error variance for such a combined estimate can be expressed as

$$e_{\mathrm{DP}} = w_{\mathrm{D}} e_{\mathrm{D}} + w_{\mathrm{P}} e_{\mathrm{P}}, \tag{41}$$

$$\sigma^2_{\delta\theta} = \left(w^2_{\mathrm{D}} \mathrm{GNR}^{-1}_{\mathrm{D}} + w^2_{\mathrm{P}} \mathrm{GNR}^{-1}_{\mathrm{P}}\right) B^{\mathrm{Design}}_{\theta}, \tag{42}$$

where w denotes the weight applied to each estimate and the subscripts D and P denote data and pilot signals, respectively.

Equating the partial derivative of (42) with respect to w_{D} to zero and noting that $w_{\mathrm{D}} + w_{\mathrm{P}} = 1$, the (rather intuitive) set of weights which minimize the tracking jitter can be shown to be

$$\{w_{\mathrm{D}}, w_{\mathrm{P}}\} = \left\{\frac{\mathrm{GNR}_{\mathrm{D}}}{\mathrm{GNR}_{\mathrm{D}} + \mathrm{GNR}_{\mathrm{P}}}, \frac{\mathrm{GNR}_{\mathrm{P}}}{\mathrm{GNR}_{\mathrm{D}} + \mathrm{GNR}_{\mathrm{P}}}\right\}. \tag{43}$$

It is worth commenting that this result differs from previously reported [10, 14] weighting guidelines which recommend that weights are chosen based upon discriminator variance. Variance-based weighting is inappropriate for some discriminators, such as the arctangent discriminator, as the variance saturates to a moderate value for low SNR$_c$ while the gain continues to reduce. Variance alone, therefore, does not reflect the true usefulness of the discriminator. GNR-based weights, as prescribed by (43), consider both gain and variance and, thus, yield superior performance. Note also that (43) implicitly considers the coherent integration period, which does not need to be equal for both the data and the pilot signals, as the GNR is a direct function of T_L.

Thus, a data/pilot architecture employing (43) should choose the appropriate discriminator for each of the pilot and data signals separately, based on the prevailing SNR$_c$ and using the guidelines presented in Section 5.2. Subsequently, the combining weights should be calculated based on the GNR values of each of the chosen discriminators. This composite phase error estimate can then be passed to the loop filter.

Note that for very low C/N_0 conditions the receivers estimate of SNR$_c$ can become noisy and unreliable, as shown in Section 5.3. Thus, in certain cases, it may be beneficial to consider alternative architectures; for example, the pilot-only approach which neglects e_{D} entirely [10]. Alternatively, the weights can be formed based upon T_L. Noting that, under high-C/N_0 conditions, the GNR becomes approximately linearly proportional to T_L, the weights could be computed by replacing GNR in (43) with the coherent integration period of the corresponding signal.

To examine their relative performance, the attenuated IF data was processed with each of a pilot-only PLL and both a time-based and a GNR-based combining PLL. A critically

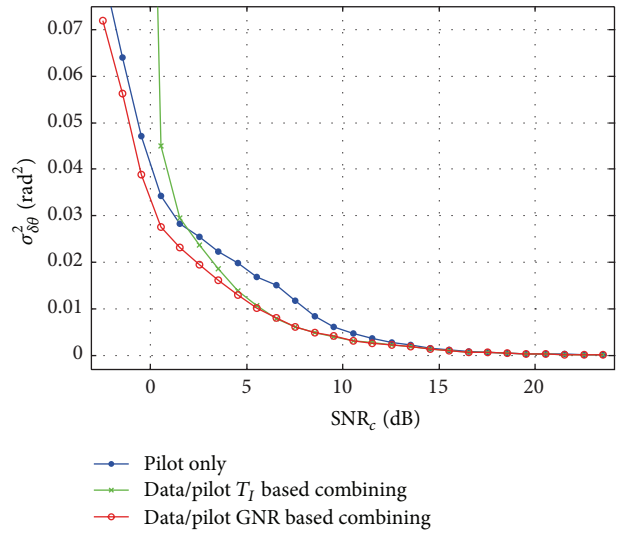

FIGURE 12: $\sigma^2_{\delta\theta}$ versus SNR$_c$ for $B_\theta^{\text{Design}} = 8$ Hz and each of the three approaches to data-pilot tracking. For this experiment, $T_L = 4$ ms and, therfore, C/N_0 (dB Hz) $\approx$ SNR$_c$ (dB) + 21.

damped, 10 Hz loop was employed in all cases, and a coherent integration period of 4 ms was used. The attenuation was time-varying, beginning at 0 dB and increasing at a rate of 0.1 dB/s to a final value of 30 dB at five minutes. The variance of the difference between the carrier phase of the attenuated data and that of the reference was calculated over a 30 second window for each PLL configuration. A plot of the measured tracking error variance versus the average SNR$_c$ over each 30 second window is shown in Figure 12.

It is clear from the measured results that when appropriate weighting is employed, the GNR-based data/pilot PLL outperforms both of the other candidate architectures, specifically in the range $0 \leq$ SNR$_c$ ≤ 10 dB reaching almost 3 dB. Perhaps more interesting, however, is the relative performance of the pilot-only and the time-based data/pilot schemes. For SNR$_c$ values higher than 5 dB, the time-based and GNR-based architectures perform equally well. This is because the arctangent and four-quadrant arctangent have equal GNR in this region, and the weights in each case are equal. Indeed, the divergence in performance at SNR$_c = 5$ dB coincides with the divergence in GNR shown in Figure 4, for very low SNR$_c$ values, the respective performance of the pilot-only and that of the GNR-based PLL converge. At this point, the difference in GNR between the pure-PLL, used for the pilot signal, and Costas, used for the data signal, is so large that w_D is almost zero.

A number of conclusions can be drawn from this experiment. Firstly, it is clear that there may always be an advantage to utilizing the data-signal for carrier phase estimation, provided the estimate can be appropriately weighted.

However, it is evident that the incremental benefit diminishes rapidly for very weak-signals, becoming effectively useless for SNR$_c$ values below approximately 0 dB. This observation is broadly in line with that of [10], which claim that a pilot-only scheme is optimal under weak-signal conditions.

It is evident, however, that inappropriate weighting can prove detrimental to receiver performance. Specifically, this occurs under low-SNR$_c$ conditions, as evidenced by the performance of the time-based combining architecture which can perform more poorly than a pilot-only PLL. Secondly, it is clear that a reasonably well-performing suboptimal architecture may be constructed by simply using a time-based combining data-pilot PLL for strong and moderate signal strengths and a pilot-only PLL when the signal is weak. An appropriate threshold may, for example, be SNR$_c \approx 3$ dB (i.e., $C/N_0 \approx 24$ dB Hz for $T_L = 4$ ms).

6. Conclusions

Following a thorough analysis of carrier phase discriminators, it is evident that, under weak-signal conditions, traditional performance models fail to fully describe PLL behavior. Both Monte-Carlo simulation and live signal tests appear to confirm that SNR$_c$-induced gain degradation is prevalent in some of these discriminators and that that has a significant impact on overall PLL performance. For the specific case of pedestrian navigation, it appears that the proposed gain-compensation technique can provide substantial performance improvements in terms of dynamic response and cycle-slip frequency.

Results pertaining to the closed loop noise performance of the PLL, when operating in its linear region, illustrated that the GNR represents a useful metric which can infer the relative closed loop performance of various discriminators, based on their respective open loop characteristics. Utilizing both this metric and the linear region analysis, experiments have confirmed that the choice of discriminator should consider the prevailing SNR$_c$, via the discriminator-specific GNR function. Moreover, in terms of the design of data/pilot tracking architectures the usefulness of the GNR metric in providing a discriminator weighting scheme appears to provide a corresponding improvement in tracking accuracy.

It is noteworthy that while the analysis presented here considered only four discriminators, the metrics, and the theoretical model employed (K_D, GNR, and LR), can be extended to consider and provide a comparative analysis of a host of carrier phase estimators. Given an expression for these three metrics as a function of SNR$_c$, this analysis could be extended to consider any memory-less discriminator.

Appendix

As the integral expressions for the statistics of the four-quadrant arctangent and the arctangent carrier phase discriminators do not appear to yield a closed form, a set of approximate expressions are presented here. The forms of the expressions have been chosen by inspection of numerical evaluations (9) and (10), for each discriminator and the coefficients (c_1, c_2, c_3) have been optimized to minimize the r.m.s error in the range -15 dB $<$ SNR$_c$ < 30 dB. Detailed also are the maximum error, max(err) of the approximate model, the value of SNR$_c$ at which this error occurs, and the standard deviation of the percentage error, denoted by σ_{Err}, calculated across the entire fit range.

The gain, K_D, and variance, $\mathrm{Var}[n^\theta]$, of the four-quadrant arctangent carrier phase discriminator can be well approximated by

$$K_D \approx \mathrm{erf}\left(c_1\sqrt{\mathrm{SNR}_c}\right), \tag{A.1}$$

where $c_1 = 0.9567$ and model errors are $\sigma_{\mathrm{Err}} = 2.883\%$, and $\mathrm{Err}_{\max} = 8.192\%$ at $\mathrm{SNR}_c = -15$ dB and

$$\mathrm{Var}\left[n^\theta\right] \approx \frac{\left(c_1 e^{-c_2\sqrt{\mathrm{SNR}_c}} + 1\right)\mathrm{erf}\left(c_3\mathrm{SNR}_c\right)}{\mathrm{SNR}_c}, \tag{A.2}$$

where $c_1 = 5.6503$, $c_2 = 1.2766$, and $c_3 = 0.4682$ and model errors are $\sigma_{\mathrm{Err}} = 2.457\%$ and $\mathrm{Err}_{\max} = 5.969\%$ at $\mathrm{SNR}_c = 4.7$ dB. Similarly, the gain, K_D, and variance, $\mathrm{Var}[n^\theta]$, of the arctangent carrier phase discriminator can be well approximated by

$$K_D \approx 1 - e^{-c_1\mathrm{SNR}_c}, \tag{A.3}$$

where $c_1 = 0.5$ and model errors are $\sigma_{\mathrm{Err}} = 3.6e^{-8}\%$ and $\mathrm{Err}_{\max} = 8.4e^{-8}\%$ at $\mathrm{SNR}_c = -15$ dB and

$$\mathrm{Var}\left[n^\theta\right] \approx \frac{\left(e^{-c_1\sqrt{\mathrm{SNR}_c}} + 1\right)\mathrm{erf}\left(c_2\mathrm{SNR}_c\right)}{\mathrm{SNR}_c}, \tag{A.4}$$

where $c_1 = 0.8046$ and $c_2 = 0.3977$ and model errors are $\sigma_{\mathrm{Err}} = 2.247\%$ and $\mathrm{Err}_{\max} = 5.530\%$ at $\mathrm{SNR}_c = 4$ dB. Approximate expressions for the GNR of the arctangent discriminators can be found by substituting the above expressions into (34). One further interesting result is the solution to (36), given the filter (8) and $P = 1$. This expresses the bandwidth of a second-order PLL which uses a proportional and integral controller and is given by

$$B_\theta = \frac{2A_0^2K_D + A_1\left(2 + A_0K_DT_L\right)}{A_0\left(4 - K_DT_L\left(2A_0 + A_1T_L\right)\right)}. \tag{A.5}$$

Explicit design equations for seconder-order filters can be found in, for example, [5, 6].

Conflict of Interests

The author declares that there is no conflict of interests regarding the publication of this paper.

References

[1] H. de Bellescize, "La réception synchrone," *L'Onde Électrique*, vol. 11, pp. 230–240, 1932.

[2] J. P. Costas, "Synchronous communications," *Proceedings of the IRE*, vol. 44, no. 12, pp. 1713–1718, 1956.

[3] J. T. Curran, D. Borio, G. Lachapelle, and C. C. Murphy, "Reducing front-end bandwidth may improve digital GNSS receiver performance," *IEEE Transactions on Signal Processing*, vol. 58, no. 4, pp. 2399–2404, 2010.

[4] W. Zhuang, "Performance analysis of GPS carrier phase observable," *IEEE Transactions on Aerospace and Electronic Systems*, vol. 32, no. 2, pp. 754–767, 1996.

[5] S. A. Stephens and J. B. Thomas, "Controlled-root formulation for digital phase-locked loops," *IEEE Transactions on Aerospace and Electronic Systems*, vol. 31, no. 1, pp. 78–95, 1995.

[6] J. T. Curran, G. Lachapelle, and C. C. Murphy, "Improving the design of frequency lock loops for GNSS receivers," *IEEE Transactions on Aerospace and Electronic Systems*, vol. 48, no. 1, pp. 850–868, 2012.

[7] J. G. Proakis, *Digital Communications*, Electrical Engineering Series, McGraw Hill International Editions, 3rd edition, 1995.

[8] E. D. Kaplan, Ed., *Understanding GPS: Principles and Applications*, vol. 1, chapter 5, Artech House, 2006.

[9] W. Hagmann and J. Habermann, "On the phase error distribution of an open loop phase estimator," in *Proceedings of the IEEE International Conference on Communications (ICC '88)*, vol. 2, pp. 1031–1037, IEEE, Philadelphia, Pa, USA, June 1988.

[10] O. Julien, "Carrier-phase tracking of future data/pilot signals," in *Proceedings of the 18th International Technical Meeting of the Satellite Division of The Institute of Navigation (ION GNSS '05)*, pp. 113–124, Long Beach, Calif, USA, September 2005.

[11] A. J. Van Dierendonck, "GPS receivers," in *Global Positioning System: Theory & Applications*, vol. 1 of *Progress in Astronautics and Aeronautics*, chapter 8, pp. 329–408, AIAA (American Institute of Aeronautics & Astronautics), 1996.

[12] A. Viterbi, "Phase-locked loop dynamics in the presence of noise by fokker-planck techniques," *Proceedings of the IEEE*, vol. 51, no. 12, pp. 1737–1753, 1963.

[13] F. M. Gardner, *Phaselock Techniques*, Wiley, 3rd edition, 2005.

[14] A. Jovanovic, Y. Tawk, C. Botteron, and P.-A. Farine, "Dual channel optimization of tracking schemes for E1 CBOC signal," in *Proceedings of the Vehicular Technology Conference (VTC Fall '11)*, pp. 1–5, IEEE, San Francisco, Calif, USA, September 2011.

[15] Vectron International, "Temperature Compensated Crystal Oscillator: Low G-Sensitivity," July 2010, http://www.vectron.com/products/tcxo/tx-508.pdf.

[16] P. Groves, *Principles of GNSS, Inertial, and Multisensor Integrated Navigation Systems*, Artech House, Boston, Mass, USA, 2013.

[17] GPS Creations, "GPS-1A," January 2012, http://www.gpscreations.com/Products GPS1A.html.

[18] Antcom Corporation, "GPS L1/L2 Antenna P/N2DG1215A-MNS-4," http://www.antcom.com/.

[19] R. L. Filler, "The acceleration sensitivity of quartz crystal oscillators: a review," *IEEE Transactions on Ultrasonics, Ferroelectrics, and Frequency Control*, vol. 35, no. 3, pp. 297–305, 1987.

[20] K. J. Åström and B. Wittenmark, *Adaptive Control*, chapter 9, Addison-Wesley, 1989.

[21] Q. Ladetto, V. Gabaglio, and B. Merminod, "Combining gyroscopes, magnetic compass and GPS for pedestrian navigation," in *Proceedings of the International Symposium on Kinematic Systems in Geodesy, Geomatics and Navigation*, pp. 205–212, Banff, Canada, August-September 2001.

[22] S. Satyanarayana, D. Borio, and G. Lachapelle, "C/N0 estimation: design criteria and reliability analysis under global navigation satellite system (GNSS) weak signal scenarios," *IET Radar, Sonar and Navigation*, vol. 6, no. 2, pp. 81–89, 2012.

[23] N. S. Alagha, "Cramer-Rao bounds of SNR estimates for BPSK and QPSK modulated signals," *IEEE Communications Letters*, vol. 5, no. 1, pp. 10–12, 2001.